A least squares linear fit of the data in the space of $(1 - \alpha_{Sm/Nd})^{-1}$ versus $(1 - k_{U/Th})^{-1}$ yields values for the two expressions in brackets. Given D_{Sm} and D_{Nd}, D_U and D_{Th} are uniquely determined and F can be calculated from Eqs. 1 and 4.

23. T. Z. La Tourrette and D. S. Burnett, *Earth Planet. Sci. Lett.* **110**, 227 (1992).
24. P. Beattie, *Nature* **363**, 63 (1993); *Earth Planet. Sci.* **117**, 379 (1993).
25. For modal melting, the concentration of an element in the liquid (C_L^A) produced by fractional melting (that is, perfect Raleigh distillation) at a given F is given by (*10*):

$$C_L^A = \frac{C_0^A}{D_A}(1 - F)^{(1/D_A - 1)} \quad (7)$$

where C_A^0 is the concentration in the original source and D_A is the bulk partition coefficient. As with batch melting (for example, Eqs. 1 and 4), $k_{U/Th}$ and $\alpha_{Sm/Nd}$ can be expressed in terms of the ratio of two fractional melting equations.

26. The mineral weight fractions used for spinel lherzolite are as follows: olivine, 59%; orthopyroxene, 21%; clinopyroxene, 8%; and spinel, 12%; those used for garnet lherzolite are: olivine, 59%; orthopyroxene, 21%; clinopyroxene, 8%; and garnet, 12%. This yields for a spinel lherzolite source: $D_U = 7.2 \times 10^{-5}$, $D_{Th} = 1.04 \times 10^{-4}$, $D_{Nd} = 0.014$, and $D_{Sm} = 0.022$. For a garnet lherzolite source the values are: $D_U = 1.2 \times 10^{-3}$, $D_{Th} = 3.0 \times 10^{-4}$, $D_{Nd} = 0.023$, and $D_{Sm} = 0.044$ (*12, 23, 24*).
27. R. W. Williams and J. B. Gill, *Geochim. Cosmochim. Acta* **53**, 1607 (1989).
28. E. R. Oxburgh, in *Physics of Magmatic Processes*, R. B. Hargraves, Ed. (Princeton Univ. Press, Princeton, NJ, 1980), pp. 161–199; M. Spieglman and D. McKenzie, *Earth Planet. Sci. Lett.* **83**, 137 (1987); D. McKenzie and M. J. Bickle, *J. Petrol.* **29**, 625 (1988).
29. Estimates of D_U, D_{Th}, and F, from our correlation of batch melting equations, depend on the selected values of D_{Sm} and D_{Nd}, which in our models are assumed to be constant. Changing the D_{Nd} and D_{Sm} values by ±20% would change the calculated F value by ±50% and the calculated D_U and D_{Th} by $\pm 3 \times 10^{-5}$ and $\pm 5 \times 10^{-5}$, respectively.
30. S. Watson and D. McKenzie, *J. Petrol.* **32**, 501 (1991).
31. N. M. Ribe, *Earth Planet. Sci. Lett.* **88**, 37 (1988).
32. A. S. Cohen and R. K. O'Nions, *ibid.* **120**, 169 (1993).
33. K.W.W.S. thanks E. Sklar, I. Carmichael, R. Jeanloz, and D. Pickett for valuable discussions pertaining to this project and T. Owens, D. Rokop, and P. Dixon for advice on matters pertaining to mass spectrometry. We also thank the anonymous reviewers. Support for this research was provided by grants from the Institute of Geophysics and Planetary Physics at Los Alamos National Laboratory, from Basic Energy Science, U.S. Department of Energy, and from the National Science Foundation (grant EAR93-04419).

17 August 1994; accepted 17 November 1994

Structural Basis for Sugar Translocation Through Maltoporin Channels at 3.1 Å Resolution

Tilman Schirmer,* Thomas A. Keller,† Yan-Fei Wang, Jurg P. Rosenbusch

Trimeric maltoporin (LamB protein) facilitates the diffusion of maltodextrins across the outer membrane of Gram-negative bacteria. The crystal structure of maltoporin from *Escherichia coli*, determined to a resolution of 3.1 angstroms, reveals an 18-stranded, antiparallel β-barrel that forms the framework of the channel. Three inwardly folded loops contribute to a constriction about halfway through the channel. Six contingent aromatic residues line the channel and form a path from the vestibule to the periplasmic outlet. Soaking of a crystal with maltotriose revealed binding of the sugar to this hydrophobic track across the constriction, which suggests that maltose and linear oligosaccharides may be translocated across the membrane by guided diffusion along this path.

Maltoporin (*1*), originally discovered as the receptor of bacteriophage λ (*2*), forms three water-filled channels across the outer membrane of Gram-negative bacteria (*3*). The maltoporin gene *lamB* (*4*) is part of the maltose regulon (*5*), which encodes the other proteins required for uptake and metabolism of maltose and linear maltooligosaccharides. For maltoporin, a sugar binding site with a dissociation constant of 10^{-4} M has been postulated (*6, 7*).

Crystals of maltoporin from *E. coli* containing one trimer in the asymmetric unit (Table 1) were obtained as described (*8*). The structure was solved by a native Patterson correlation method (*9*), yielding the position of the local triad, followed by molecular averaging. After phase extension from 8 to 3.1 Å resolution, the resulting map was of high quality and allowed the entire polypeptide chain of 421 residues to be traced. The model has been partially refined with strict noncrystallographic symmetry constraints (*10*).

The scaffold of the monomer (Fig. 1) is an 18-stranded antiparallel β barrel forming a channel. Strands are connected to their nearest neighbors by long loops and turns. The loops are found at the end of the barrel that is exposed to the cell exterior. Three of them (L1, L3, and L6; Fig. 1) fold into the barrel and are, together with loop L2 from an adjacent subunit, packed against the inner wall of the barrel and line the channel. The remaining loops form a compact structure at the cell surface.

Subunit interactions within the stable trimer structure (Fig. 2) involve peripheral contacts between L1 and L5, in addition to large parts of the barrel and loop L2 close to the molecular symmetry axis. A hydrophobic area encircles the trimer laterally and would match the core of the membrane in vivo. It is formed predominantly by short aliphatic residues. Eleven of those 14 transmembrane β strands that contribute to this area are flanked by aromatic residues at the nonpolar-polar boundary. Three polar residues, Asn^{228}, Asp^{274}, and Tyr^{288}, are also located within the hydrophobic zone. Their compatibility with the environment of low dielectric constant is likely due to saturation of their hydrogen-bonding potential by mutual interactions. Resemblance of the maltoporin fold to that of nonspecific porins is obvious, although there is no detectable sequence homology, and nonspecific porins are about 80 residues shorter and form 16-stranded barrels with a single internal

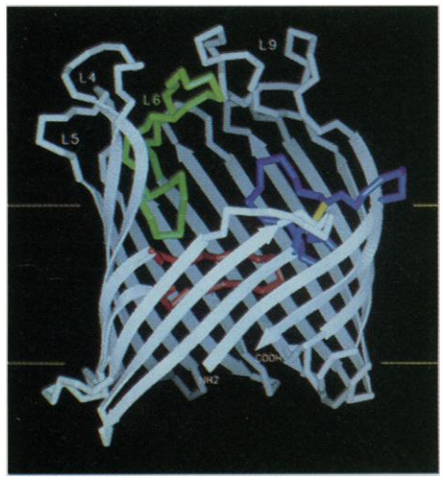

Fig. 1. Schematic drawing of the maltoporin monomer. The cell exterior is at the top and the periplasmic space is at the bottom. The area of the subunit involved in trimer contacts is facing the viewer. The 18 antiparallel β strands of the barrel [shear number (*24*) = 22] are represented by arrows. Strands are connected to their nearest neighbors by loops or regular turns (*25*). Loops L1 (blue), L3 (red), and L6 (green) fold inward toward the barrel (see also Fig. 3A). L3 (red) is the major determinant of the constriction site. The yellow bond symbolizes the disulfide bridge Cys^{22}-Cys^{38} within L1. Loop L2 (facing the viewer) latches onto an adjacent subunit in the trimer. Loops L4 to L6 and L9 form a large protrusion. The horizontal lines delineate the boundaries of the hydrophobic core of the membrane as inferred from the hydrophobic area found on the molecular surface. All figures were prepared with the program O (*23*).

T. Schirmer, Department of Structural Biology, Biozentrum, University of Basel, CH-4056 Basel, Switzerland.
T. A. Keller, Y.-F. Wang, J. P. Rosenbusch, Department of Microbiology, Biozentrum, University of Basel, CH-4056 Basel, Switzerland.

*To whom correspondence should be addressed.
†Present address: Ecole Polytechnique Fédérale, Institut de Chimie Physique, CH-1015 Lausanne, Switzerland.

loop (*11*, *12*). In particular, the asymmetric distribution of loops and turns, the location of the chain termini at the subunit interface, and the role of L2 and L3 are similar.

The assignments of cell-surface exposed loops deduced from biochemical and genetic data (*13*) are entirely consistent with our three-dimensional structure. In the inferred topology model, the orientations of more than half of the transmembrane β strands, however, are incorrect. A recently reported topology based on the recognition of hydropathic and aromatic patterns (*14*) correctly identified locations and polarities of 16 of the 18 strands.

The protuberances on the extracellular surface of the trimer (Fig. 2) shield the three pores and harbor the point mutations in strains selected for bacteriophage resistance (*15*). Only about half of the sites involved in recognition by phage λ are exposed (Fig. 2), whereas the remaining sites appear to be buried at locations where the loops pack together to form the protrusions. Such mutations might indirectly cause structural alterations on the surface, or they might affect the dynamic behavior of the loops. In any event, structural variations of the protrusion may protect the molecule from recognition by harmful agents (such as phages, antibodies, and proteases) without affecting its function.

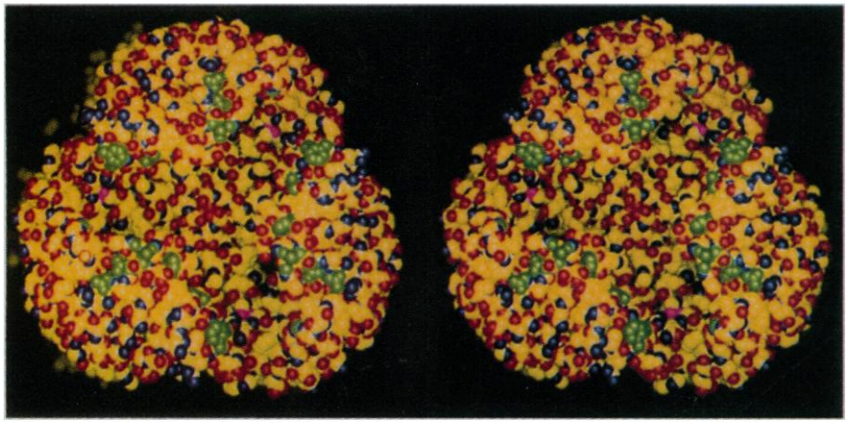

Fig. 2. Space-filling stereo representation of the maltoporin trimer. The view is toward the face exposed to the cell surface and along the symmetry axis. The protrusions at the periphery (loops L4 to L6 and L9) convey the impression of a half-open "tulip" and largely conceal the three transmembrane channels. Carbon, nitrogen, and oxygen atoms are shown in yellow, blue, and red, respectively. The sulfur atoms (pink) of the disulfide bridge can be seen at the bottom of the vestibule. Sites of mutations that confer resistance to phage λ (*15*) are highlighted in green. Their residue numbers are 155, 164, 259, 386, 387, 394, and 401. Additional sites conveying resistance are buried within the structure of the protrusion (see text).

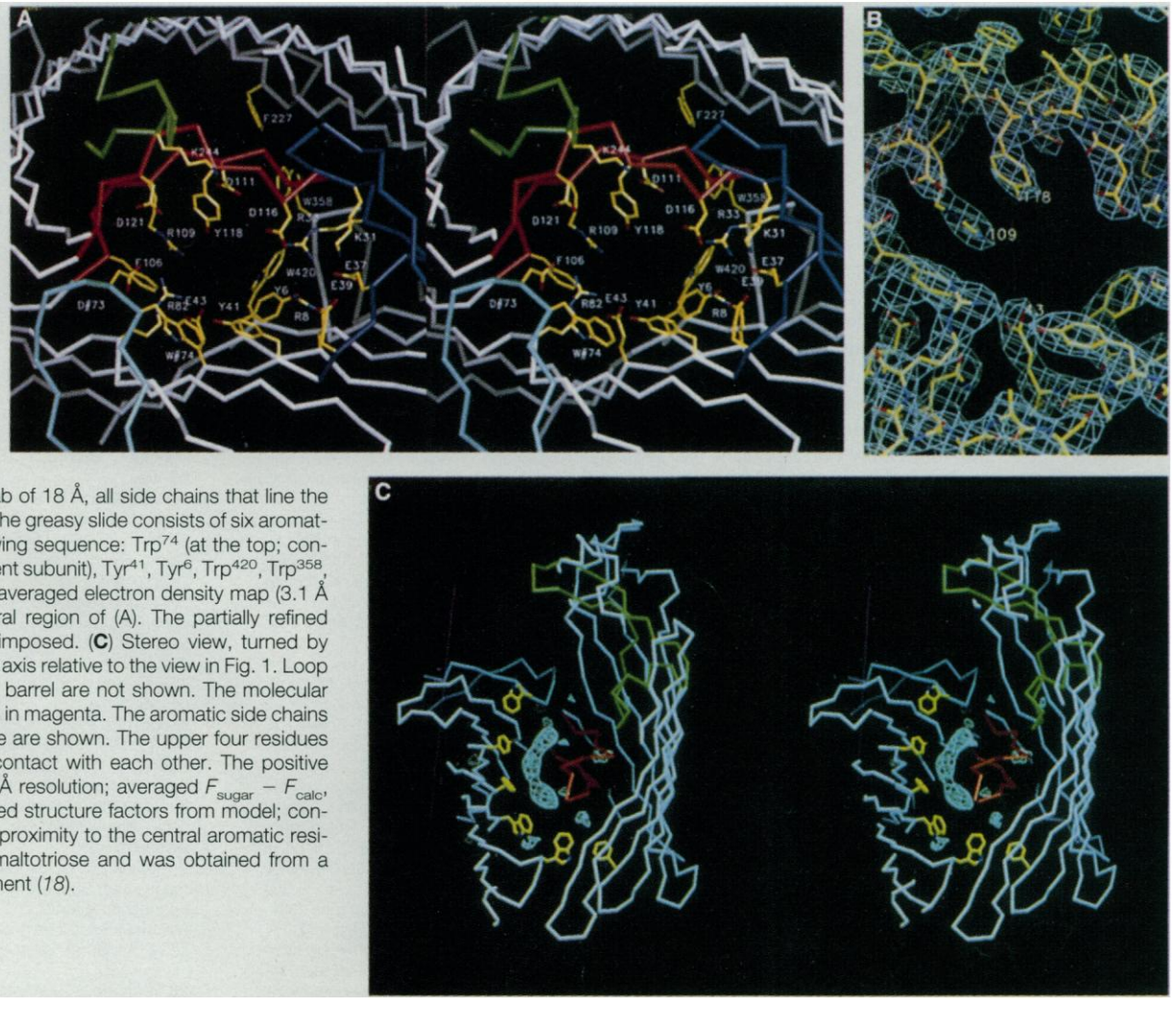

Fig. 3. The structure of the channel. For the C_α trace, the same color code was used as in Fig. 1. Loop L2 from an adjacent monomer, which also contributes to the channel, is shown in light blue. (**A**) Stereo diagram of the channel constriction. The direction of the view is similar to that in Fig. 2, but is zoomed in on the pore of the top monomer. For clarity, all loops obstructing this view have been clipped off. Within a slab of 18 Å, all side chains that line the channel are depicted. The greasy slide consists of six aromatic residues in the following sequence: Trp^{74} (at the top; contributed from the adjacent subunit), Tyr^{41}, Tyr^{6}, Trp^{420}, Trp^{358}, and Phe^{227}. (**B**) Cyclic averaged electron density map (3.1 Å resolution) of the central region of (A). The partially refined model is shown superimposed. (**C**) Stereo view, turned by ~90° around the barrel axis relative to the view in Fig. 1. Loop L1 and the front of the barrel are not shown. The molecular three-fold axis is shown in magenta. The aromatic side chains forming the greasy slide are shown. The upper four residues are in van der Waals contact with each other. The positive difference density (4.0 Å resolution; averaged $F_{sugar} - F_{calc}$, α_{calc} map with calculated structure factors from model; contour level, 5σ) found in proximity to the central aromatic residues corresponds to maltotriose and was obtained from a crystal-soaking experiment (*18*).

Table 1. Crystallographic data. The crystals are of orthorhombic space-group $C222_1$ (a = 131.9 Å, b = 214.8 Å, c = 220.2 Å) and contain one trimer in the asymmetric unit. Cyclic averaging was started with the use of the data between 30 and 8 Å resolution. The averaging R factor (R_{aver}) dropped from 49.4 to 27.2% during this process. Phase extension from 8 to 3.1 Å resolution was done in 53 steps with concomitant tightening of the mask. The R_{aver} of the final map was 13.1%, with a real-space correlation of 0.95. Values given in parenthesis are for the highest resolution shell.

	Native maltoporin	Maltoporin/maltotriose complex (*18*)
Detector	Image plate (MARRESEARCH)	TV detector (FAST)
Resolution range (Å)	30 to 3.1	30 to 4.0
Number of unique reflections	54,001	23,125
R_{merge} (%)*	8.8 (35.9)	13.4 (23.7)
Completeness (%)	95.3 (90.4)	89.5 (80.1)
Redundancy	3.6 (3.2)	2.4 (2.2)

*$R_{merge} = \Sigma(|I_i - \langle I \rangle|)/\Sigma\langle I \rangle$.

The constriction of the channel (Fig. 3) is located about halfway through the membrane. As in the nonspecific porins, it is defined by residues from L3 and from the juxtaposed barrel wall, but the lumen at the channel entrance is further restricted by residues from L1 and L6. The pore has a diameter of 5 to 6 Å and is thus considerably smaller than that of OmpF porin (*12*), which qualitatively explains its lower ion conductance (*16*). Only aromatic and ionizable residues occur at the channel constriction (Fig. 3A). The latter are distributed pairwise, but are in most cases too far apart to form salt bridges. The charged groups of five such pairs (for example, Arg^{109}-Glu^{43}) are separated by 4 to 6 Å, which suggests that water molecules mediate their mutual interactions.

A salient feature is a series of aromatic residues arranged along a left-handed helical path at the channel lining. They form what may be dubbed a "greasy slide" and extend from the channel vestibule through the constriction to the periplasmic outlet (Fig. 3C). Because the hydrophobic faces of glycosyl moieties are known to stack with aromatic residues in sugar-binding proteins (*17*), such an arrangement may correspond to a series of sugar-binding sites. Indeed, soaking of a maltoporin crystal in maltotriose solution (*18*) revealed positive difference density for the trisaccharide close to the aromatic residues at the center of the channel (Fig. 3C). The translocation of small sugars may thus be envisaged as a process that is initiated by binding of the solute to the aromatic subsites at the pore entrance. This would align the substrate with respect to the pore axis and would be followed by guided diffusion along the greasy slide through the narrow constriction. Longer maltooligosaccharides may relax their intrinsic helical conformation (*19*) to enable interactions with several of the subsites. Because the distances between the aromatic groups (6 to 7 Å) are larger than those between the glycosyl residues in maltodextrins (5 Å), tight binding to all subsites with unfavorable rates of dissociation would be avoided.

Residue Tyr^{118} and the ionizable residues (Fig. 3A) in the vicinity of the greasy slide are located in such a way that they are likely to interact with the hydroxyl groups of the sugar (thereby replacing the hydration shells). This presumably accounts for the sugar specificity of the channel. The positions of all mutations selected for altered affinities toward maltodextrin (*20*) cluster at the pore constriction. Elucidation of the structures of maltoporin and selected mutants, free or in complex with sugars of different lengths, will now, in conjunction with functional analyses, allow a rigorous testing of the mechanism suggested by the structure presented here.

REFERENCES AND NOTES

1. C. Wandersman, M. Schwartz, T. Ferenci, *J. Bacteriol.* **140**, 1 (1979); M. Luckey and H. Nikaido, *Proc. Natl. Acad. Sci. U.S.A.* **77**, 167 (1980); T. Ferenci, *Bioessays* **10**, 3 (1989).
2. L. Randall-Hazelbauer and M. Schwartz, *J. Bacteriol.* **116**, 1436 (1973).
3. J.-M. Neuhaus, H. Schindler, J. P. Rosenbusch, *EMBO J.* **2**, 1987 (1983).
4. J.-M. Clément and M. Hofnung, *Cell* **27**, 507 (1981).
5. M. Schwartz, in Escherichia coli *and* Salmonella typhimurium: *Cellular and Molecular Biology*, F. C. Neidhardt, Ed. (American Society of Microbiology, Washington, DC, 1987), pp. 1482–1502.
6. R. Benz, A. Schmid, H. Greetje, H. Vos-Scheperkeuter, *J. Membr. Biol.* **100**, 21 (1987); S. Freundlieb, U. Ehmann, W. Boos, *J. Biol. Chem.* **263**, 314 (1988); K. Gehring, C.-H. Cheng, H. Nikaido, B. K. Jap, *J. Bacteriol.* **173**, 1873 (1991).
7. B. Dargent, J. P. Rosenbusch, F. Pattus, *FEBS Lett.* **220**, 136 (1987).
8. R. M. Garavito, U. Hinz, J.-M. Neuhaus, *J. Biol. Chem.* **259**, 4254 (1984); K. A. Stauffer, M. G. P. Page, A. Hardmeyer, T. A. Keller, R. A. Pauptit, *J. Mol. Biol.* **211**, 297 (1990); T. A. Keller, T. Ferenci, A. Prilipov, J. P. Rosenbusch, *Biochem. Biophys. Res. Comm.* **199**, 767 (1994).
9. The self-rotation function indicated approximate alignment of the local triad with the cell axis c. Crystal packing considerations have previously yielded a tentative packing (*21*) that is now confirmed. The local threefold symmetry axis has direction cosines −0.108, 0.000, and 0.99415, and intersects the crystallographic twofold rotation axis that runs parallel to b at right angles at the point (x, y, z) = (0.1 Å, 36.0 Å, 54.05 Å). Hexamers of 32 point-group symmetry are generated with the trimers in eclipsed orientation with respect to each other. There is a local screw axis (direction = 0.500, −0.866, 0.000; κ = 169°) that relates trimers from adjacent hexamers. Its screw component t was determined by the Patterson correlation method (local translation function) as described by Rossmann and colleagues [M. G. Rossmann, D. M. Blow, M. M. Harding, E. Coller, *Acta Crystallogr.* **17**, 338 (1964)], but operating in Patterson space with the averaging routines RAVE (*22*). In the crystals, the position of the local triad is directly related to t. A clear signal (correlation = 0.16; peak height, 3.6 σ above mean; second highest peak, 1.3 σ above mean) was obtained in a one-dimensional scan at t = 62 Å, and hence the position of the triad was determined. The OmpF porin trimer model (*12*) was centered on the local triad with the azimuthal orientation as obtained earlier (*21*) and with a distance of 26 Å from the dyad. This model yielded start phases (30 to 8 Å; random R factor) and served to generate a mask for cyclic three-fold averaging with the use of RAVE (*22*). Refinement of the local transformations proved to be critical.
10. The final averaged map was of high quality, and model building (*23*) was straightforward, which was also reflected in the R factor of 34.2% of the initial model. Conventional positional refinement and restrained B factor refinement with strict noncrystallographic constraints with the use of the program X-PLOR [A. T. Brünger, *X-PLOR Version 2.1* (Yale University, New Haven, CT, 1990)] reduced the R factor (15 to 3.1 Å) to 22.1% (R_{free} = 25.1%). The root mean square deviations from ideal bond lengths and angles were 0.026 Å and 2.6°, respectively.
11. M. S. Weiss *et al.*, *Science* **254**, 1627 (1991); A. Kreusch, E. Neubüser, E. Schiltz, J. Weckesser, G. E. Schulz, *Protein Sci.* **3**, 58 (1994).
12. S. W. Cowan *et al.*, *Nature* **358**, 727 (1992).
13. A. Charbit, J. Ronco, V. Michel, C. Werts, M. Hofnung, *J. Bacteriol.* **173**, 262 (1991).
14. T. Schirmer and S. W. Cowan, *Protein Sci.* **2**, 1361 (1993).
15. A. Charbit, K. Gehring, H. Nikaido, T. Ferenci, M. Hofnung, *J. Mol. Biol.* **201**, 487 (1988).
16. The ion conductance of maltoporin is 0.15 nS (*7*) as compared with 0.8 nS for OmpF porin [L. K. Buehler, S. Kusumoto, H. Zhang, J. P. Rosenbusch, *J. Biol. Chem.* **266**, 24446 (1991)].
17. J. C. Spurlino, G.-Y. Lu, F. A. Quiocho, *ibid.*, p. 5202.
18. A maltoporin crystal was soaked in 1 mM maltotriose for 10 days.
19. E. Goldsmith, S. Sprang, R. Flettrick, *J. Mol. Biol.* **156**, 411 (1982).
20. T. Ferenci and K.-S. Lee, *ibid.* **160**, 431 (1982). The mutants show residue replacements at positions 8, 74, 82, 118, and 121 [H. G. Heine, J. Kyngdon, T. Ferenci, *Gene* **53**, 287 (1987)]; see also Fig. 3A.
21. R. A. Pauptit *et al.*, *J. Struct. Biol.* **107**, 136 (1991).
22. G.J. Kleywegt and T.A. Jones, "Halloween . . . Masks and Bones," in *From First Map to Final Model*, S. Bailey, R. Hubbard, D. Waller, Eds. (SERC Daresbury Laboratory, Daresbury, UK, 1994), pp. 59–65.
23. T. A. Jones and M. Kjeldgaard, *O—The Manual* (Uppsala University, Sweden, 1991).
24. A. M. Lesk, C.-I. Brändén, C. Chothia, *Proteins Struct. Funct. Genet.* **5**, 139 (1989).
25. Segments folded into loop or turn structures at the cell-surface exposed end of the barrel contain residues 16 to 39 (loop L1), 69 to 79 (L2), 106 to 123 (L3), 149 to 166 (L4), 198 to 209 (L5), 239 to 265 (L6), 299 to 301 (L7), 335 to 337 (L8), and 375 to 405 (L9). On the periplasmic end of the barrel, the connecting turns and loops are defined by residues 51 to 56, 91 to 97, 135 to 136, 180 to 183, 224 to 225, 281 to 282, 317 to 319, and 352 to 361. A β bulge in β6 (the side chains of Glu^{130} and Asn^{131} both protrude toward the periplasmic exit hall) perturbs the regularity of the hydropathicity pattern and has earlier prevented prediction of this transmembrane segment (*14*).

26. We thank our colleagues for critical reading of the manuscript. Support by the Swiss National Science Foundation (grants to T.S. and J.P.R.) is gratefully acknowledged. The coordinates have been deposited in the Brookhaven Protein Databank.

28 September 1994; accepted 2 December 1994